OUKA
The University of Osaka
Institutional Knowledge Archive

Title	Molecular dynamics study on the effects of cuboid nanostructure on the distribution of local thermal resistance at a solid-liquid interface
Author(s)	Omori, Takuto; Shibahara, Masahiko
Citation	International Journal of Thermal Sciences. 2025, 215, p. 109949
Version Type	VoR
URL	https://hdl.handle.net/11094/102198
rights	This article is licensed under a Creative Commons Attribution-NonCommercial-NoDerivatives 4.0 International License.
Note	

The University of Osaka Institutional Knowledge Archive : OUKA

https://ir.library.osaka-u.ac.jp/

The University of Osaka

International Journal of Thermal Sciences 215 (2025) 109949

Contents lists available at ScienceDirect

International Journal of Thermal Sciences

journal homepage: www.elsevier.com/locate/ijts

Molecular dynamics study on the effects of cuboid nanostructure on the distribution of local thermal resistance at a solid–liquid interface

Takuto Omori *, Masahiko Shibahara

Department of Mechanical Engineering, Graduate School of Engineering, Osaka University, 2-1 Yamadaoka, Suita, 565-0871, Osaka, Japan

ARTICLE INFO

Keywords:
Molecular dynamics
Interfacial thermal resistance
Solid–liquid interface
Nanostructure

ABSTRACT

This study focuses on thermal transport at the interface between solid and liquid with various cuboid nanostructure systems. We calculated the solid–liquid interfacial thermal resistance (ITR) and the distribution of local ITRs with a 0.2 nm spatial resolution. The results were obtained using non–equilibrium molecular dynamics. Applying a thermal circuit model, we computed the thermal resistance by combining the local ITRs. Also, we introduced spectral analysis to explain the distribution of local ITR magnitudes. As a result, we found that the local ITRs decreased at the top corner of the nanostructure and increased at its base. The thermal transport at the top corner contributed significantly to the total thermal transport at the solid–liquid interface. It was revealed that the ratio of the overall ITR to the combined local ITRs agreed with the ratio of the area of a flat surface to the area along the lower wall and the nanostructure, including the Cassie–Baxter state, only when the local temperature jumps around the interface are closely similar i.e. the interaction strength between solid and liquid is not extremely high. Moreover, from spectral analysis of solid atoms, we found that the vibrational density of states (VDOS) and the spectral heat flux of the solid atoms at the top corner of the nanostructure peaked in a low–frequency range and the VDOS overlap became higher at the top corner in all cases. This strong vibrational coupling is another factor contributing to the lowest local ITR at the top corner of the nanostructure.

1. Introduction

In recent years, due to the miniaturization and densification of electric devices, properties of physical quantities such as thermal transport have attracted attention at the nanoscale [1,2] because they are crucial for thermal management in microdevices [3,4]. Numerous technologies have been developed utilizing thermal transport between different materials, such as heat exchangers in air conditioners and heat sinks in electronic devices [5–7]. Therefore, it is highly desired across various fields to improve the performance of these devices related to thermal transport [8]. The interfacial thermal resistance (ITR) becomes dominant at the nanoscale, thus it is essential to understand the ITR in detail in order to elucidate the thermal transport mechanisms at the solid–liquid interface. It is known that the ITR significantly influences the overall thermal resistance compared to the thermal resistance of the material themselves [9]. Nanoscale analysis of the thermal transport at a solid–liquid interface began with a study on the Kapitza length [10]. There is a substantial temperature difference (also called "temperature jump") at the solid–liquid interface, sufficient to interfere with energy or phonon transport [11]. These characteristics at the interface contribute to the motivation for facilitating interfacial thermal transport [12].

Up to now, researchers have conducted a lot of experimental investigations on microscale thermal transport. Ulman [13] reported that the wettability was controlled by a coating of self–assembled monolayers (SAMs). Due to the influence of the SAMs, the interaction strength between solid and liquid changes. A similar study by Tian et al. [14] revealed that the interfacial thermal conductance (ITC), which is the reciprocal of ITR, became large due to the influence of the coated solid surface. Wilson et al. [15] suggested that the ITC between hydrophilic gold nanoparticles and water was within a factor of 2 of theoretical estimates based on the diffuse–mismatch model. Recent research using a thermal circuit model (TCM) at the macroscale proved that a designed thermal circuit could be utilized for the reliability analysis of the heat sink under long–term load profiles when the thermal dissipation performance decreases [16]. The authors modeled the effects of impurities on the heartsink's thermal dissipation performance using the TCM as several tunable thermal resistances whose value can be adjusted according to the impurity distribution and demonstrated that the temperature of heat sinks can be accurately and quickly estimated

* Corresponding author.
E-mail address: omori@mte.mech.eng.osaka-u.ac.jp (T. Omori).

https://doi.org/10.1016/j.ijthermalsci.2025.109949
Received 23 December 2024; Received in revised form 3 March 2025; Accepted 17 April 2025
Available online 1 May 2025
1290-0729/© 2025 The Authors. Published by Elsevier Masson SAS. This is an open access article under the CC BY-NC-ND license (http://creativecommons.org/licenses/by-nc-nd/4.0/).

under various reliability conditions. For TCM applications on a smaller scale, Ishii et al. [17] modeled the change in resistance due to a phase change and revealed that the phase change model could be expressed by connecting three models with different melting points and latent heat amounts in parallel resulting in validation of the experimental measured and calculated values.

Since it is challenging to experimentally investigate the thermal transport characteristics at the nanoscale over nanoseconds, many studies using the molecular dynamics (MD) method have been reported [18–20]. Those studies have calculated the ITRs by MD. Using MD simulations, it was shown that the ITR of the interfacial region decreased as the nanostructure gaps became narrower [21]. Gao et al. [22] investigated the effect of mechanical interfaces with sub–nm roughness and concluded that the maximum change in ITC is about 21 times even at the same root–mean–square roughness. Shibahara et al. [23] researched the effects of nanostructural clearances on ITR. They utilized a classical MD simulation in the case of the Lennard–Jones (LJ) liquid and found that in the case of a modified surface at the nanoscale, the ITR is dependent on the potential parameter between liquid molecules and nanostructure atoms itself rather than the geometric surface area. Qu et al. [24] found that introducing a 0.5–nm–thick amorphous–silicon layer increases the ITC between silicon and diamond by more than 38% compared to that between silicon and diamond without the amorphous–silicon layer. Also, they revealed that the increase of the ITC with increasing temperature can be mainly attributed to the scattering between inelastic phonons at the interface. Ueki et al. [25] reported that a layer of hydrophilic nanoparticles was able to decrease the solid–liquid ITR. It has become evident that vibrational properties are a significant factor in thermal transport at the nanoscale [26]. Wei et al. [27] investigated the interfacial thermal transport through adsorption clusters and discovered that the vibration frequencies become dominant in thermal transport with the increase of adsorption amount. Fujiwara et al. [28] suggested that a structured surface in the atomic scale can alter the magnitude of the overall ITR, which leads to altering the spectra of thermal transport at the interface. According to El–Rifai et al. [29], the vibrational density of states (VDOS) exhibits the availability of frequency range, and the spectral heat flux (SHF) expresses the utilization of those for thermal transport. Also, they reported that a greater increase in the utilization of the mid–high frequency range caused a "crossover" in the relationship between the ITC and the interaction strength between solid and liquid.

A study using a calculation model in the Cassie–Baxter (CB) state showed that the ITC of larger grooves and hydrophobic states became low and the ITC of the groove surface in a hydrophilic state was approximately twice that of the flat surface [30]. The ITR increased as the nanostructure gap became narrower due to the CB state [21]. Jiang et al. [31] used TCMs to predict ITRs between water and a nanostructure surface in the case of the CB state and found that the TCMs accurately forecast the ITRs of nanostructure surfaces in Cu–water systems. Another study has investigated the local ITR with a 0.2 nm spatial distribution [32]. Due to the existence of the nanostructure on a surface, the overall ITR decreased and the spatial distribution of local ITR fluctuated corresponding to the interaction strength between solid and liquid. By using the TCM, they revealed that the overall ITR agreed with the combined local ITRs within certain errors considering the magnification ratio of the surface area. Also, the relationship between the coupling of vibrational properties and local ITRs was investigated. However, the reason why the two ITRs do not completely agree or whether those ITRs match in the case of different sizes of nanostructure and the case of the CB state is still not fully understood.

Based on the above, the objective of the present study is to investigate the general relationship between the overall ITR and the local ITR in detail by applying non–equilibrium molecular dynamics (NEMD) simulation with a cuboid–structured surface at the atomic scale. In the present study, we calculate the local thermal transport with a spatial distribution of 0.2 nm using MD simulations of both the Wenzel (W) and CB state. To understand the influence of local ITRs and the relationship between the overall ITR and the combined local ITRs for nanoscale engineering, we employed the Pt–Ar system since it allows us to observe simple thermal transport process at the nanoscale. Subsequently, the relationship between the local ITRs and the interaction strength between solid and liquid is investigated in detail. The reason why the ratio of the overall ITR to the combined local ITRs agrees with the ratio of a flat surface area to the area along the bottom wall and the nanostructure within certain errors has been investigated by altering the nanostructure size and the number of liquid molecules between the nanostructures. Moreover, vibrational properties at the solid–liquid interface are also computed to investigate the influence of local ITRs.

2. Simulation methods

In the present study, we employed the three calculation systems shown in Fig. 1. In these systems, liquid argon molecules are sandwiched between solid platinum walls. Three different cuboid nanostructures indicated as "Slit (I)", "Slit (II)" and "Slit (III)" were installed on the lower wall surface. Slit (I) has a nanoslit with a size of $1.57\times1.57\times3.92$ nm^3, Slit (II) has a nanoslit with a size of $2.74\times1.57\times3.92$ nm^3, and in the case of Slit (III), Pt atoms in a row in the middle of the lower wall surface, which is the smallest possible cuboid structure. For the purposes of this study, we refer to Slit (III) as an "adatom system". Slit (II) was mainly used to observe the CB state, which is the case where few fluid molecules exist between the nanostructures. Since we built Slit (III) based on a flat surface model, the system length in the z direction of Slit (III) is shorter than those of Slit (I) and Slit (II). The intermolecular forces were calculated using the 12–6 LJ potential [33] as described in Eq. (1)

$$\phi_{ij}(r_{ij}) = 4\alpha\varepsilon_{ij}\left\{\left(\frac{\sigma_{ij}}{r_{ij}}\right)^{12} - \left(\frac{\sigma_{ij}}{r_{ij}}\right)^{6}\right\} \tag{1}$$

where ε_{ij} and σ_{ij} are LJ parameters, and r_{ij} is an intermolecular distance between two particles [34,35].

We used a cut–off distance of 3.3σ. An interaction strength parameter α was introduced to represent different interaction strengths between Pt and Ar. For calculations between homogeneous particles, α was considered to be unity. In the case of Slit (I), we altered the value of α from 0.05 to 0.3. In general, $\alpha = 0.05$ corresponds to the wettability of an argon droplet on a platinum crystal surface with contact angles $\theta = 100°$ and a value of $\alpha = 0.1$ corresponds to that of $\theta = 0°$ [36]. Thus, α greater than 0.1 represents an extremely strong adsorption of liquid molecules as chemisorption. We set it to 0.1 for the upper wall and 0.03 for the lower wall in the case of Slit (II) to achieve the CB state. Also, in the case of Slit (III), we set it from 0.04 to 0.3. The leap–frog method was used for numerical integration with a time step of 2 fs. Periodic boundary conditions were applied in the x and y directions, while the outermost layers of both walls were fixed in the z direction. Solid walls and a nanostructure were arranged in the face-centered cubic crystal of Pt. Liquid molecules are in contact with the surface (1 0 0) lattice plane on the upper and lower walls and the top surface of the nanostructure, and with the surface (0 1 0) plane on the sides of the nanostructure. We adjusted the pressure of the calculation system to approximately 10 MPa by controlling the number of Ar molecules in the system. The exception was when we observed the CB state in the case of Slit (II), when the pressure was set to 1.3 MPa. Temperature control of the solid wall was performed by the Langevin method, which allows to generate a constant temperature gradient in the z direction. The temperatures of the upper and lower walls were set to 130 K and 80 K, respectively. A steady state was achieved through calculations for over 2 ns. Subsequently, we acquired the calculation data on various physical quantities for 10 ns.

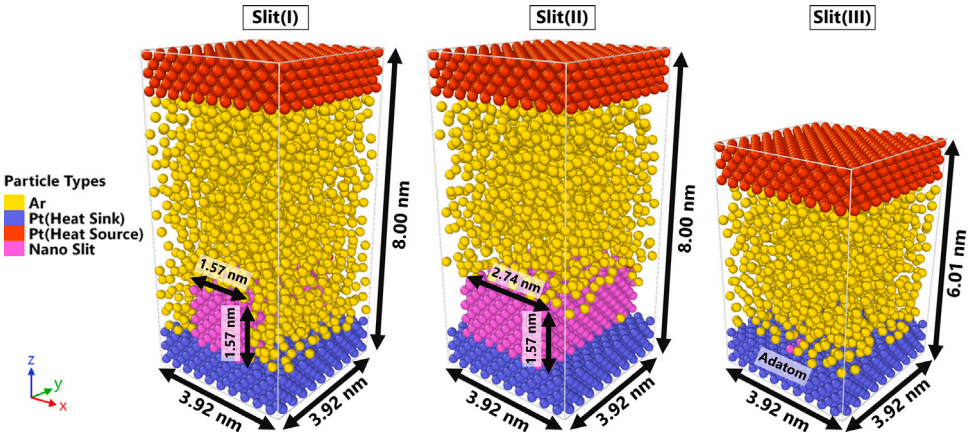

Fig. 1. Snapshots of calculation systems.

2.1. Interfacial thermal resistance

When the overall ITR is defined in the same manner as a thermal resistance in general thermal engineering, the following equation holds:

$$R_{\mathrm{th}} = \Delta T / q \tag{2}$$

where R_{th} [$\mathrm{m^2K/W}$] represents the overall ITR, ΔT [K] represents the difference between the temperatures of solid and liquid at an interface, and q [$\mathrm{W/m^2}$] represents the heat flux across the solid–liquid interface. The overall temperature difference is obtained by extrapolating the temperature distributions of liquid and solid from the bulk–like region, where the interaction force on liquid molecules from solid atoms becomes extremely small compared to that between liquid molecules, and from the second solid layer from the Langevin layer, respectively, to a distance equivalent to one quarter of the Pt lattice constant away from the initial solid configuration. Similarly to the overall ITR, we calculated the local ITRs to investigate local thermal transport along the solid–liquid interface with a nanostructure in detail. The local ITR at the local interface k is defined as below.

$$R_k = \Delta T_k / q_k \tag{3}$$

where ΔT_k [K] represents the local temperature difference, and q_k [$\mathrm{W/m^2}$] represents the local heat flux. Local solid–liquid interfaces are defined as shown in Fig. 2. Similar to the previous study [32], with a spatial resolution of about 0.2 nm, 32 local solid–liquid interfaces were introduced along the lower wall and the nanostructure in the case of Slit (I) and Slit (II). The area of local interfaces is 0.2×3.9 $\mathrm{nm^2}$ (shown in green) except that of the top corner. The area of the top corner of the nanostructure is twice the area of others (shown in red). In the case of Slit (III), the local area at the position of the adatom is defined to be the same as the areas of other local interfaces (shown in green) and there are 20 local interfaces in total. Further, the local temperature difference was calculated by using the average temperature of solid atoms and that of liquid molecules contacting with the local interface. In the present study, each local temperature of both solid and liquid is obtained with a spatial distribution of 0.2 nm. A local heat flux is distributed at a local interface where the line segment connecting pairs of solid atoms and liquid molecules intersects as shown in Fig. 3. First, consider a line segment connecting an Ar molecule and a Pt atom pair interacting with each other (purple arrowhead). Then, find the intersection with the line segment representing the solid–liquid interface is calculated. Finally, determine which local interface the intersection of the two line segments belongs to. Only for the local heat flux at the adatom in the case of Slit (III), the local heat flux is calculated by the local thermal transport received by the adatoms since we considered the Slit (III) system has almost the same contact area of the bottom wall as that of the flat surface model.

When applying the TCM, these local ITRs can be assumed to form a parallel thermal circuit as shown in Fig. 4. Therefore, considering the area of the local interface and the area along the lower wall and the nanostructure, the thermal resistance combined with local ITRs is calculated by

$$R_{\mathrm{cir}} = \frac{A_{\mathrm{nano}}}{\sum_k A_k / R_k} \tag{4}$$

where A_{nano} [$\mathrm{m^2}$] is the area along the lower wall and the nanostructure, A_k [$\mathrm{m^2}$] is the area of the local interface, and R_k [$\mathrm{m^2K/W}$] is the local thermal resistance. If the total thermal transport at each local interface agrees with the total thermal transport within the whole system, the following Eq. (5) holds.

$$\frac{R_{\mathrm{th}}}{R_{\mathrm{cir}}} = \frac{A_{\mathrm{flat}}}{A_{\mathrm{nano}}} \tag{5}$$

where A_{flat} [$\mathrm{m^2}$] represents the area of the flat surface of the solid wall. Although it was reported that Eq. (5) held in the specific cases of the W state [32], it still needs to be verified whether this relationship holds generally by using calculation results of various nanostructure interfaces in MD simulations. For this reason, we conducted simulations in the case of different structure sizes and CB states.

2.2. Vibrational properties

For further understanding of the local thermal transport, we calculated the VDOS of both liquid molecules and solid atoms. The VDOS is obtained by applying a Fourier transform to the velocity autocorrelation function [37] as

$$\mathrm{VDOS}(\omega) = C \int_0^\infty \langle \boldsymbol{v}(\tau) \cdot \boldsymbol{v}(0) \rangle \exp(i\omega\tau) \mathrm{d}\tau \tag{6}$$

where ω [rad/s] is the angular frequency, and $\boldsymbol{v}$ [m/s] is the velocity vector of the particle. By multiplying by C, the integral of VDOS is normalized to one [38]. The VDOS overlap between solid and liquid is calculated as follows [38]:

$$\mathrm{Overlap} = \int \min[\mathrm{VDOS_S}(\omega),\ \mathrm{VDOS_L}(\omega)] \mathrm{d}\omega \tag{7}$$

where $\mathrm{VDOS_S}$ and $\mathrm{VDOS_L}$ express the VDOS of solid atoms and liquid molecules, respectively, and min[ ] is the smaller element between values in the bracket.

Moreover, a SHF [26,28] was introduced to analyze the vibrational properties of thermal transport at a solid–liquid interface. In the present study, the local SHF across the interface k was calculated by

$$q_{\mathrm{L}_k \to \mathrm{S}_k}(\omega) = \frac{2}{A_k} \mathrm{Re} \sum_{i \in \mathrm{S}_k} \sum_{j \in \mathrm{L}_k} \int_{-\infty}^{\infty} \langle \boldsymbol{v}_i(0) \cdot \boldsymbol{F}_{ij}(\tau) \rangle \exp(i\omega\tau) \mathrm{d}\tau \tag{8}$$

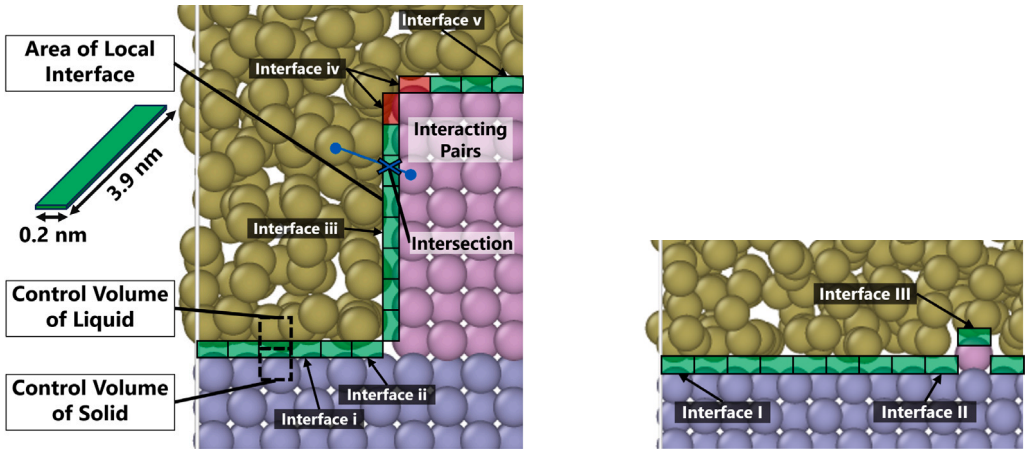

(a) Slit (I) and Slit (Ⅱ) (b) Slit (Ⅲ)

Fig. 2. Schematic diagram of local interfaces.

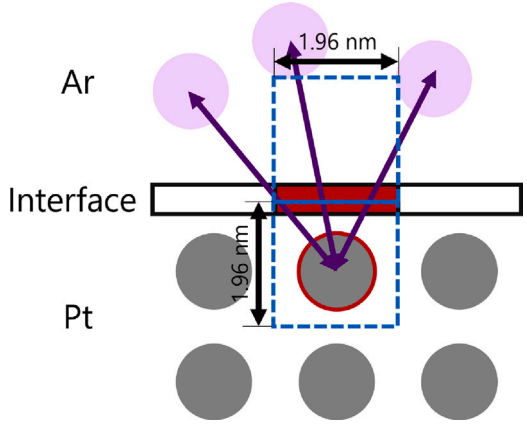

Fig. 3. Schematic diagram of calculation method of local heat flux.

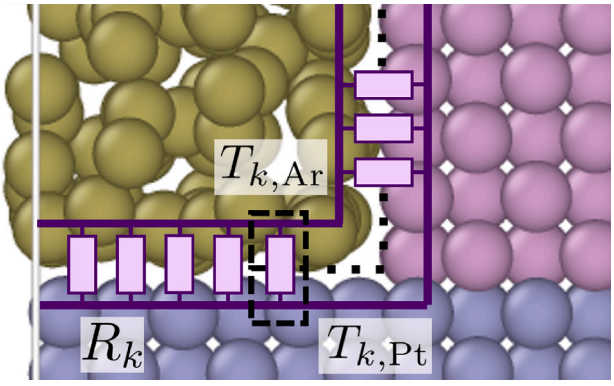

Fig. 4. Schematic diagram of a thermal circuit along the interface.

where A_k is the area of a local interface k, $\boldsymbol{v}_i$ is the velocity vector of a solid atom i, $\boldsymbol{F}_{ij}$ is the force vector received by a solid atom i from a liquid molecule j. S_k and L_k represent the group of particles deployed to the local interface k where the line segment connecting pairs of solid atom and liquid molecule intersects [32].

3. Results and discussions

3.1. Distributions of temperature and density of liquid

We calculated the two–dimensional (2D) temperature distribution of the liquid and its one-dimensional (1D) density and temperature distributions. In the 2D distributions in the xz plane, the density of each control volume $0.2 \times 3.9 \times 0.2$ nm^3 is obtained by time–averaging for 10 ns. The 1D distributions are also calculated by time–averaging over regions in which the entire system is divided into 300 control volumes in the z direction. The results for the Slit (I) system are shown in Figs. 5(a)–5(c) and 6(a)–6(c), those of the CB state in the case of Slit (II) are shown in Figs. 5(d) and 6(d), and those in the case of Slit (III) are indicated in Figs. 5(e)–5(f) and 6(e)–6(f). It is observed that the number of liquid molecules adsorbed to the solid wall increased as α became larger. Accordingly, the gradient of the temperature distribution increased. From the 2D temperature distribution, we can confirm that the temperature of the liquid gradually decreases from the upper wall to the lower wall. In the case of the CB state, the density of the liquid is extremely low in the region below $z = 3.0$ nm, and we can confirm that few Ar molecules exist between the nanostructures. In addition, the temperature gradient became small in the case of the CB state since the ITR greatly increased due to the absence of fluid molecules between the nanostructures. There were some local temperature fluctuations, but when we calculate for a longer time, such fluctuations of local temperature are expected to become much smaller. Considering the limitation of calculation time and the result of one–dimensional temperature gradient in Figs. 5(a)–5(f), we determined that the systems were in a steady state.

3.2. Distributions of local ITR

Fig. 7 demonstrates the distributions of the local ITRs in the cases of Slit (I) system with various α, the CB state of Slit (II) system, and Slit (III) system. To observe the distributions of local ITRs in the case of the extremely high interaction strength and reveal the conditions under which Eq. (5) holds, we calculated local ITRs in the case of $\alpha = 0.3$ for all systems. For Slit (I) and Slit (II), the local ITRs were relatively lower at the top corner of the nanostructure, and higher at its base, regardless of the interaction strength α. These characteristics agree with the results of the previous study using different sizes of nanoslit systems [32]. In the case of Slit (III), the local ITR became lower at the position of the adatom, and higher at the local interface adjacent to the adatom. One of the possible reasons for this phenomenon is that more liquid molecules per unit area surrounded solid atoms of the top corner or adatom, whereas the density near the base was relatively low. For quantitative analysis, we calculated the number of interacting Pt–Ar pairs that transport thermal energy at each local interface in the

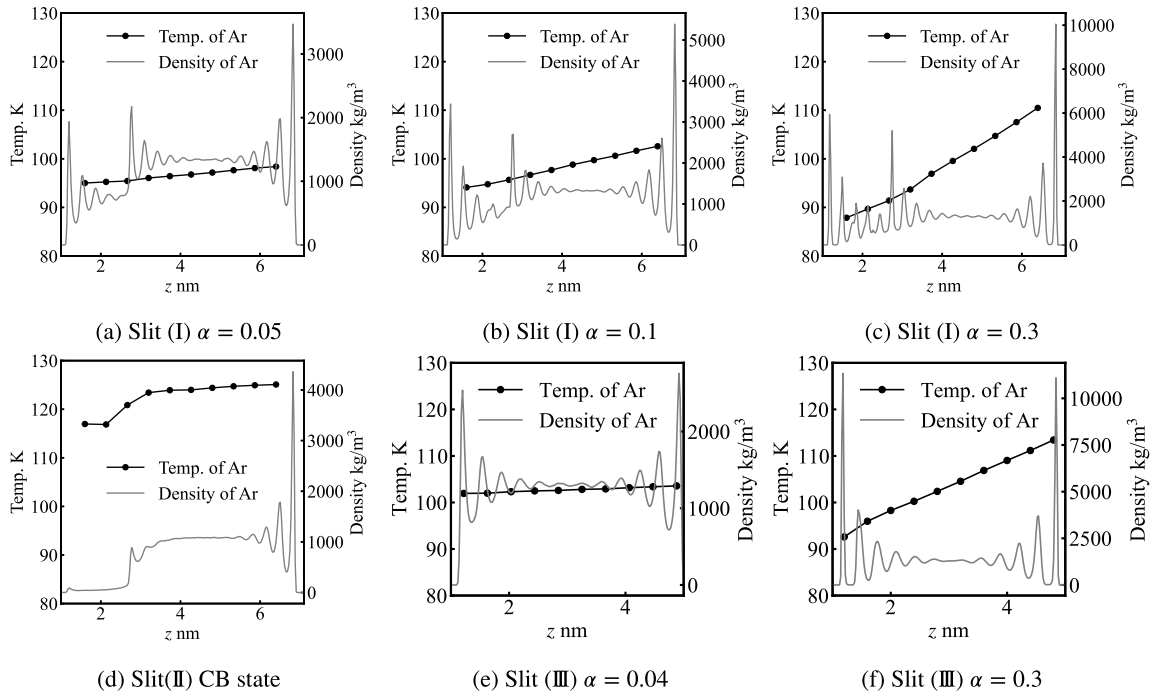

Fig. 5. Distributions of density and temperature.

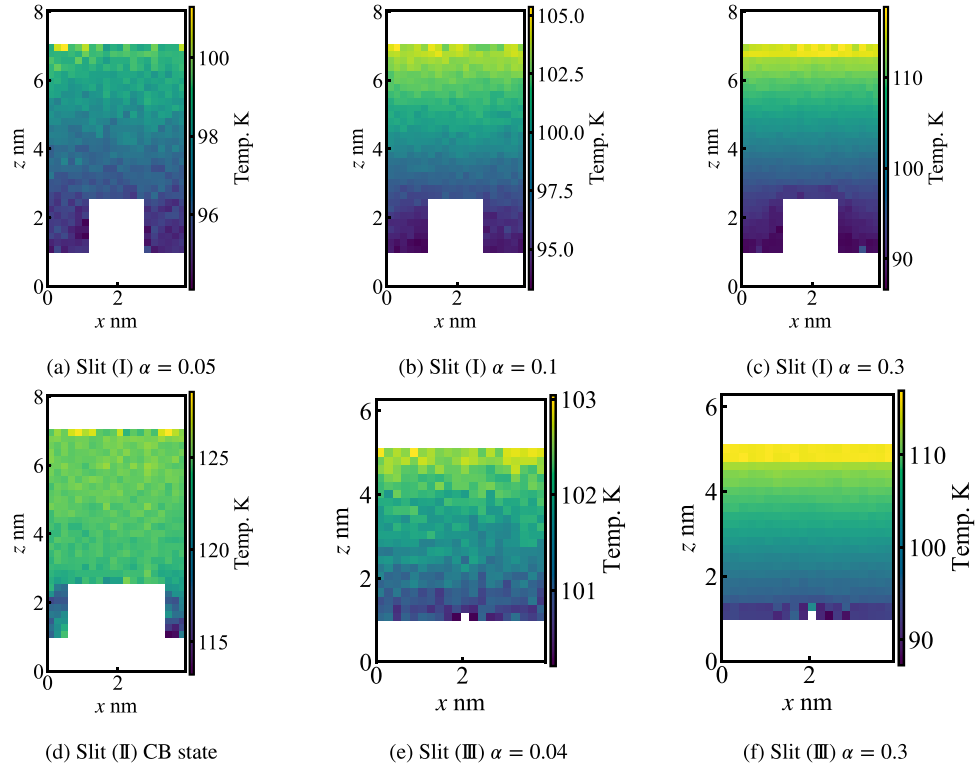

Fig. 6. 2D temperature distributions.

case of Slit (I). The results are shown in Fig. 8. We calculated the number of pairs at the top corner by doubling the local area of other local interfaces as in the method utilized to calculate the local ITRs and accumulating for the y direction. As described in Fig. 8, it is verified that the number of interacting pairs that transport thermal energy at the top corner is larger than that at other local interfaces. Although there are fewer liquid molecules around the top corner compared to the W state, in the case of the CB state the local ITR at the top corner is also lower than the ITRs of other local interfaces. Therefore, there must be another reason why the local ITR is low at the top corner in addition to the large number of liquid molecules per unit area at the top corner. Fig. 7(c) exhibits a higher value of the local ITR at $x = 0$. This is because the extremely high interaction strength leads to pronounced fluctuations of adsorbed liquid molecules at the interface. The density of liquid molecules fluctuated around the interface, thus the local ITR became larger in the region of lower density. For quantitative analysis,

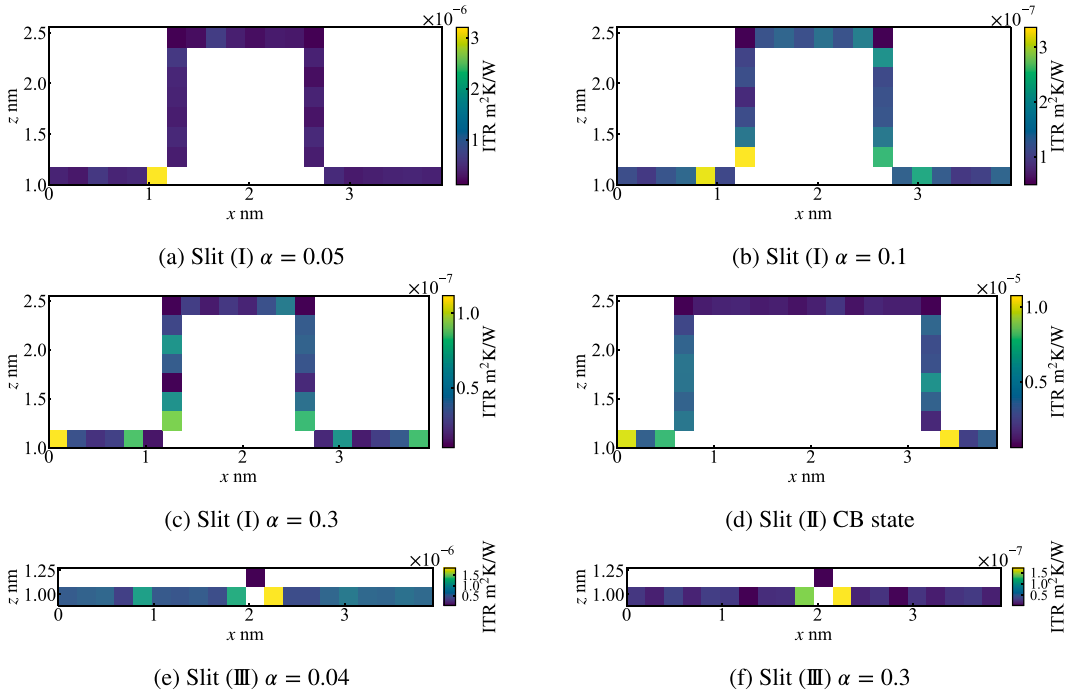

Fig. 7. Distributions of local ITRs.

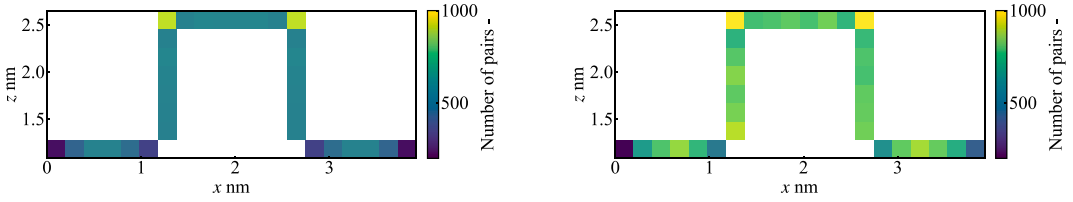

Fig. 8. Distributions of the number of interacting Pt–Ar pairs that transport thermal energy at each local interface in the case of Slit (I).

we calculated the statistical variance of the heat flux, the temperature difference, and the local ITR at the local interfaces, respectively. The results are indicated in Table 1. There were remarkable relationships between α and the variance of the three physical quantities we focused on. As the interaction strength α increased, the variance of the heat flux and the temperature difference increased. The heat flux increases with increasing α, and the ITR and the temperature difference decrease in turn. On the other hand, the variance of the temperature difference increased as α becomes larger. Therefore, it can be said that the adsorption of more liquid molecules to the solid wall enhanced the thermal transport at the interface, but it led to a greater temperature difference variance. In the case of the CB state, the variance of the heat flux became small, and that of the local ITR became large because of the lower number of liquid molecules between the nanostructures. The temperature difference between the lower wall and the liquid became large, while that between the top surface of the nanostructure and the liquid was relatively small, resulting in a large magnitude of the temperature difference variance.

Table 1
Variance of heat flux, temperature difference, and local ITR.

	Heat flux $[(W/m^2)^2]$	Temp. Difference $[(K)^2]$	Local ITR $[(m^2\ K/W)^2]$
Slit (I) $\alpha = 0.05$	5.09×10^{14}	0.226	2.56×10^{-13}
Slit (I) $\alpha = 0.1$	2.36×10^{15}	0.686	3.97×10^{-15}
Slit (I) $\alpha = 0.3$	3.44×10^{16}	3.09	6.52×10^{-16}
Slit (II) CB state	2.53×10^{14}	9.34	5.96×10^{-12}
Slit (III) $\alpha = 0.04$	7.05×10^{15}	0.419	1.23×10^{-13}
Slit (III) $\alpha = 0.3$	3.74×10^{17}	7.29	1.65×10^{-15}

3.3. Overall ITR and combined local ITRs

From the results above, we calculated the overall ITR using Eq. (2) and the combined local ITRs using Eqs. (3)–(4). Also, the ratio of the overall ITR to the combined local ITRs, which is defined as "ITR ratio", was calculated. In addition, we computed the relative error between the area ratio and the ITR ratio. The results are shown in Table 2 and Fig. 9. We calculated the ITRs of Slit (II) system in both the W and CB states for comparison, which are shown in Table 2. For all Slit (I) and (II) cases, the area ratio A_{flat}/A_{nano} equals 0.556. To confirm the validity of the calculation method used for local ITRs, we first computed the ITR ratio of the flat surface model, where the area ratio should be 1.0. We confirmed that the ITR ratio was 0.998 in the case of α = 0.04, indicating an almost complete agreement with the area ratio. However, the ITR ratio became 0.932 at α = 0.3 even in the case of the flat surface model, resulting in a relative error of 7.3%. Consequently, it can be considered that the assumption of a parallel thermal circuit may no longer hold in the case of an extremely high interaction strength between solid and liquid due to the fluctuation of the density of adsorbed liquid molecules to the solid wall. A detailed explanation of this is discussed later. From Table 2, in the case of α = 0.05 for Slit (I), we can confirm that the ITR ratio agrees with

Table 2
Comparison of the overall ITR, the combined local ITRs, ITR ratio and relative error.

	R_{th} [m^2 K/W]	R_{cir} [m^2 K/W]	R_{th}/R_{cir}	A_{flat}/A_{nano}	Error [%]
Slit (I) $\alpha = 0.05$	1.83×10^{-7}	3.44×10^{-7}	0.531		−4.53
Slit (I) $\alpha = 0.1$	5.75×10^{-8}	1.24×10^{-7}	0.464		−16.5
Slit (I) $\alpha = 0.3$	4.87×10^{-9}	2.82×10^{-8}	0.173	0.556	−68.9
Slit (II) CB state	1.05×10^{-6}	1.95×10^{-6}	0.541		−2.67
Slit (II) W state	4.71×10^{-7}	8.67×10^{-7}	0.543		−2.22
Slit (III) $\alpha = 0.04$	4.21×10^{-7}	4.10×10^{-7}	1.03	1.00	2.61
Slit (III) $\alpha = 0.3$	1.82×10^{-8}	1.83×10^{-8}	0.996		−0.01

the area ratio; the relative error is 4.5%. In the cases of Slit (II), the ITR ratio corresponds to the area ratio regardless of the CB state or W state; the relative errors are 2.7% and 2.3%, respectively. However, as α increased, the ITR ratio was not always aligned with the area ratio. In the case of $\alpha = 0.3$, the ITR ratio is approximately one–third of the area ratio. This is attributed to the increased adsorption of liquid molecules to the solid wall, which leads to the large changes in the temperature difference in local areas discussed in the previous subsection. When we assume that the parallel thermal circuit holds rigorously, the local temperature difference between solid atoms and liquid molecules must be uniform. Therefore, when the adsorption of liquid molecules to the solid surface is relatively weak, the ITR and area ratios match relatively well, whereas stronger adsorption causes the ITR ratio to deviate from the area ratio. As indicated in Fig. 9, even in the case of lower α, the ITR ratio did not perfectly agree with the area ratio. This discrepancy is also attributed to the fact that the temperature differences are not completely constant at all local interfaces. The ITR ratios of Slit (II) system of both the W state and the CB state agreed with the area ratio better than those of Slit (I) system. In the case of Slit (II) CB state, the variance of the temperature difference becomes 1.69 when focusing solely on the local area of the top surface of the nanostructure. The thermal transport via the top surface becomes dominant for the overall thermal transport at the solid–liquid interface, and the local ITR at the base of the nanostructure, where its value becomes relatively large, has a negligible impact on the combined local ITRs in the case of the CB state. As a result, even in the case of the CB state, the ITR ratio agreed with the area ratio. We confirmed a similar phenomenon in the case of Slit (III). In the case of Slit (III), the ITR ratio exceeded the area ratio in the case of $\alpha = 0.04$. This is due to the fact that the surface area is not exactly the same as that of the flat surface model. In the present study, because of the low height of the nanostructure in the case of Slit (III), we considered the surface area of Slit (III) to be the same as the flat surface model. In fact, Slit (III) has a one–atom–height nanostructure. From the above, regardless of the size of the nanostructure and the CB state, Eq. (5) is valid only when the local temperature jump around the solid–liquid interface is close to constant, i.e., when the interaction force between solid and liquid is not significantly high and the adsorption of liquid molecules to the solid is relatively weak.

3.4. Vibrational analysis

The VDOS and SHF of the entire interface and the specific local interfaces were calculated to reveal the relationship between the vibrational characteristics and the distribution of the local ITRs. We defined the five specific local interfaces in the case of Slit (I) and Slit (II) as shown in Fig. 2(a): the center of the lower wall as Interface i, the base of the nanostructure as Interface ii, the center of the sidewall of the nanostructure as Interface iii, the top corner of the nanostructure as Interface iv, and the center of the top surface of the nanostructure as Interface v. We also defined the three specific interfaces in the case of Slit (III) as shown in Fig. 2(b): the local interface at $x = 0$ as Interface I, adjacent to the adatom as Interface II and the adatom as Interface III.

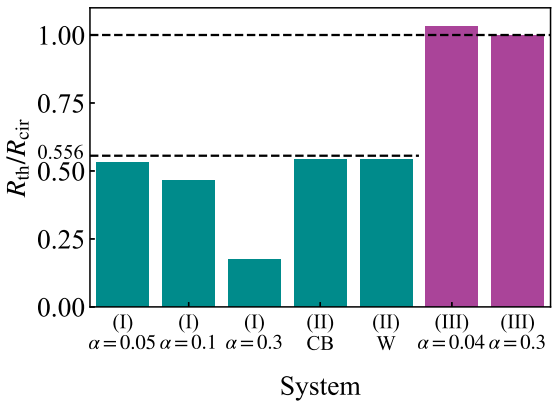

Fig. 9. Comparison of ITR ratio dependent on α and wetting states. The area ratio in the case of Slit (I) and Slit (II) is 0.556, and that in the case of Slit (III) is 1.0, respectively.

In the present study, the local VDOS and SHF were calculated for all pairs of liquid molecules and solid atoms involved in energy transport at the local interface. As typical results of the VDOS and SHF, those of the whole liquid molecules and solid atoms of the lower wall and the nanostructure in the case of Slit (I) of $\alpha = 0.1$ are shown in Fig. 10, the VDOS of solid atoms and liquid molecules at the specific interfaces are shown in Fig. 11, and the SHF of solid atoms at the specific interfaces are indicated in Fig. 12, respectively.

3.4.1. VDOS

As shown in Fig. 10, the VDOS of the liquid molecules has a peak at zero THz and decreases with increasing frequency, while that of the solid atoms has peaks over the 0–10 THz range. As indicated in Fig. 11, the local VDOS of solid atoms was not affected substantially by the interaction strength α. This implies that the VDOS of the solid atoms is not strongly influenced by the magnitude of the interaction force from the adjacent liquid molecules as reported in the previous study [32]. On the other hand, the local VDOS of liquid molecules varies with the interaction strength α between solid and liquid. Since the VDOS of the liquid has a distribution within the range of 0–5 THz, the vibrations in the same range of solid atoms can receive more energy from liquid molecules. The local VDOS of solid atoms at Interface iv has a peak at around 2 THz, while that at other interfaces tends to have peaks at around 4 THz. Therefore, the local VDOS of solid atoms at the top corner contains more contributions in lower–frequency modes than that at other interfaces. However, in the case of Slit (II) $\alpha = 0.3$, the local VDOS of liquid molecules peaked at 2–3 THz. Although the VDOS of liquid molecules generally peaked at 0 THz as shown in Fig. 10(a), the local VDOS of liquid molecules was influenced by solid atoms and shifted to the high–frequency side due to the extremely high interaction strength.

3.4.2. SHF

As shown in Fig. 12, the SHF of each local interface represents the vibrational characteristics of thermal transport and relates to the features of the VDOS of solid atoms. We confirmed that the integral of each local SHF agreed with the local thermal transport at the specific interface. The SHF at the top corner has a peak at around 2 THz in all cases. In the case of Slit (I) $\alpha = 0.3$, the SHF of all local interfaces peaked at around 4 THz except that of Interface iv. The frequency peak of 4 THz is also observed in the VDOS of the entire interface as shown in Fig. 10. Consequently, it can be considered that the solid atoms can receive thermal energy at around 4 THz from the liquid molecules absorbed to the solid wall except at the top corners. Also, in the case of $\alpha = 0.3$, the SHF at each local interface exhibits the highest peak of approximately 1.5 MW/m^2 THz. This indicates that the local thermal

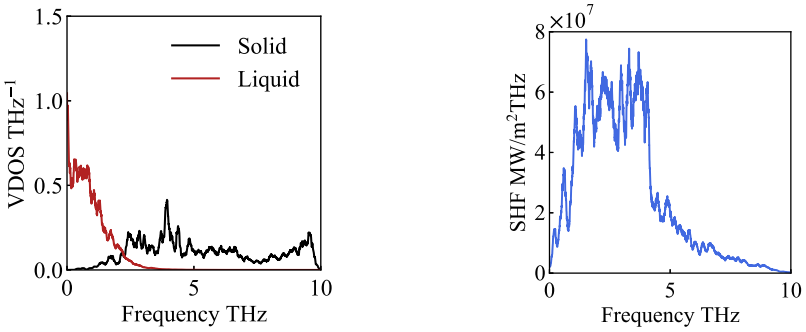

(a) VDOS (b) SHF

Fig. 10. VDOS and SHF of the entire interface.

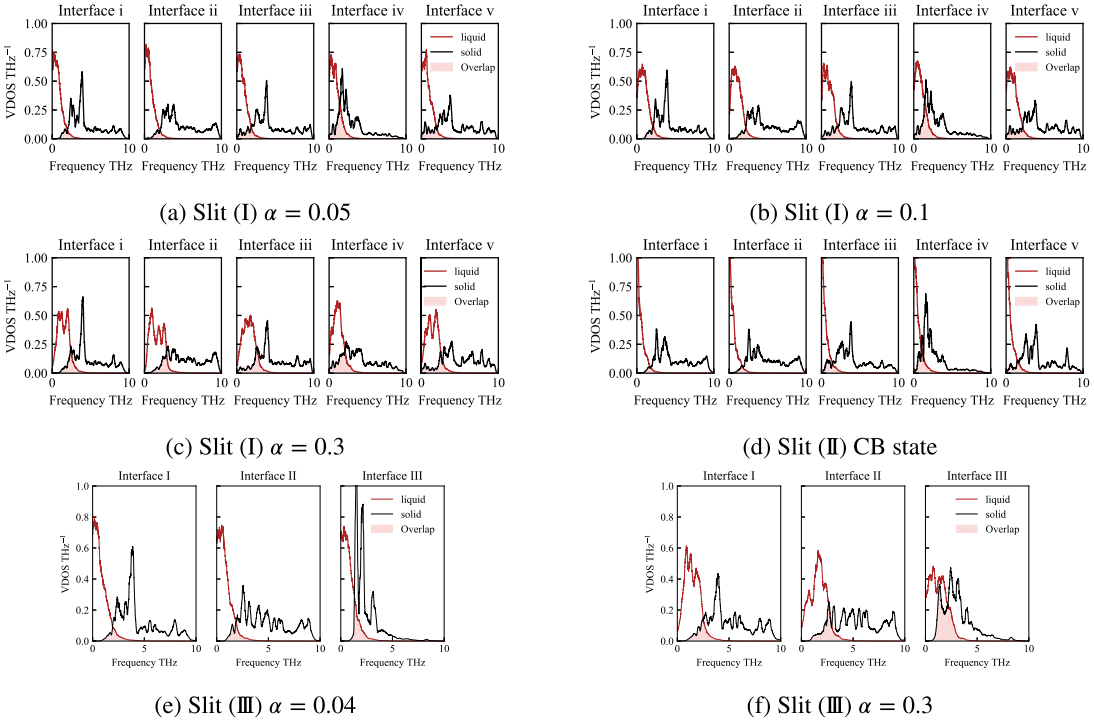

(a) Slit (I) $\alpha = 0.05$ (b) Slit (I) $\alpha = 0.1$

(c) Slit (I) $\alpha = 0.3$ (d) Slit (Ⅱ) CB state

(e) Slit (Ⅲ) $\alpha = 0.04$ (f) Slit (Ⅲ) $\alpha = 0.3$

Fig. 11. VDOS of solid atoms and liquid molecules at the specific local interfaces.

transport at the top corner is not significantly different from that at other local interfaces in the case of the extremely high interaction strength. On the other hand, in the case of the CB state, the SHF at the top corner was the most pronounced among other conditions. Also, the SHF at Interface i–iii had a narrow frequency range compared to Interface iv–v. This indicates that the thermal transport at the top corner is crucial and dominant in the case of the CB state. Furthermore, in the case of Slit (III), the SHF at Interface III has the largest peak among three specific interfaces. From this trend, we can speculate that the local thermal transport is dominated by the adatom at Interface III.

3.4.3. *VDOS overlap*

As mentioned above, the local VDOS of solid atoms at the top corner possesses the most pronounced peak at 2 THz. The impact of this appears in the VDOS overlap between solid and liquid. Fig. 13 exhibits the VDOS overlaps between solid and liquid at the specific local interfaces while the shaded areas in Fig. 11 indicate the VDOS overlap between solid and liquid at the local interface. From Fig. 13, the overlap at Interface iv had the largest value among all the specific local interfaces in the case of Slit (I) and Slit (II). In other words, the vibrational coupling is the strongest at the top corner regardless of the interaction strength. El–Rifai et al. [29] suggested that as the VDOS overlap increases, the interfacial thermal conductance becomes larger. Therefore, we consider that this is another reason why the local ITR becomes the lowest at the top corner in addition to the large number of surrounding liquid molecules. The cuboid nanostructure on the solid surface exhibits the most pronounced vibrational properties at the top corner and the adatom in addition to the expansion of contact area. In the case of the CB state, since the interaction strength between solid and liquid is relatively small and there are few liquid molecules between the nanostructures, the local ITRs become relatively large. Focusing solely on the top surface of the nanostructure, the VDOS overlap at Interface iv was relatively large compared to Interface iii and Interface v.

3.5. *Contribution of local area to overall thermal transport*

As discussed in the previous Section 3.2, the local ITR at the top corner of the cuboid nanostructure is small compared to those at other local interfaces. Unlike other local interfaces, the area of the local interface at the top corner is twice as large as that of other local interfaces (Fig. 2). Therefore, the local interface at the top corner is definitely in contact with more liquid molecules than are the other

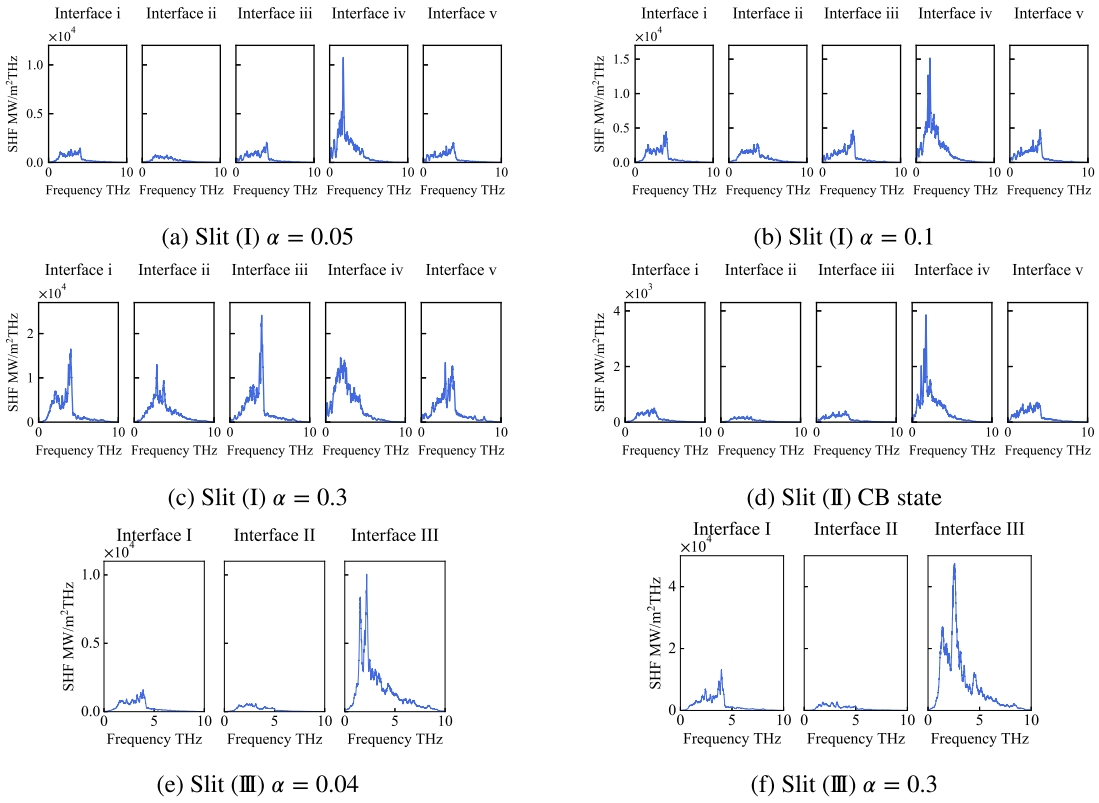

Fig. 12. SHF of solid atoms at the specific local interfaces.

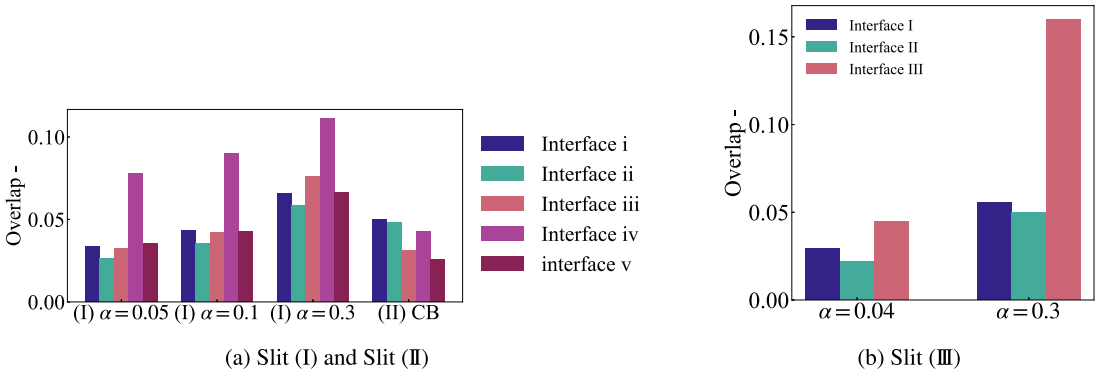

Fig. 13. VDOS overlaps between solid and liquid at the specific local interfaces.

interfaces. Although the previous study [32] has also found a low value of the local ITR at the top corner of the nanostructure, it is not described in detail how much the top corner affects the overall thermal transport compared to other local interfaces. Hence, we calculated the ratio of the local heat flux with the maximum value set to 1 to determine the extent to which the top corner affects the overall thermal transport. The results are exhibited in Fig. 14 and the ratios of the maximum to the minimum (Max/Min) are shown in Table 3. From Fig. 14, in the same way as Table 1, we found that the local heat flux became largest at the top corner of the nanostructure in all cases. As α increased, the fluctuation of local heat flux became larger. This is because the values of the local heat flux become large corresponding to increasing the interaction strength between solid and liquid. In the case of Slit (I), the local heat flux of other local interfaces is always found to be less than half of that of the top corner itself. Moreover, the local heat flux of the sidewalls of the nanostructure and the bottom wall became less than 20% of that of the top corner in the case of Slit (II). In the case of Slit (III), the local heat flux at the adatom is consistently more than ten times larger than that of other local interfaces and the Max/Min ratio became larger in the case of $\alpha = 0.3$ than that in the case of $\alpha = 0.04$. We consider this is because the magnitude of local heat flux depends on the adsorption state of liquid molecules rather than on the structural features such as the top corner or base due to the extremely small structure of adatoms. The local heat flux was exceptionally large at the top corner and at the adatom. Fujiwara and Shibahara [39] have reported that they detected heat fluxes from the adatoms to the liquid phase, not only along the macroscopic temperature gradient direction, but also in the direction normal to the temperature gradient, thus they concluded that the adatoms are significant for the enhancement of the thermal transport at the single–atom scale. As indicated in Table 3, there was no obvious relationship between α and the Max/Min ratio. In the case of Slit (II), the Max/Min ratio of the heat flux was relatively large compared to the case of Slit (I). The Max/Min ratio became the smallest in the case of $\alpha = 0.1$. We consider that this tendency on the Max/Min ratio of heat flux can be attributed to the adsorption state of liquid molecules to the solid bottom wall. Since the interaction strength

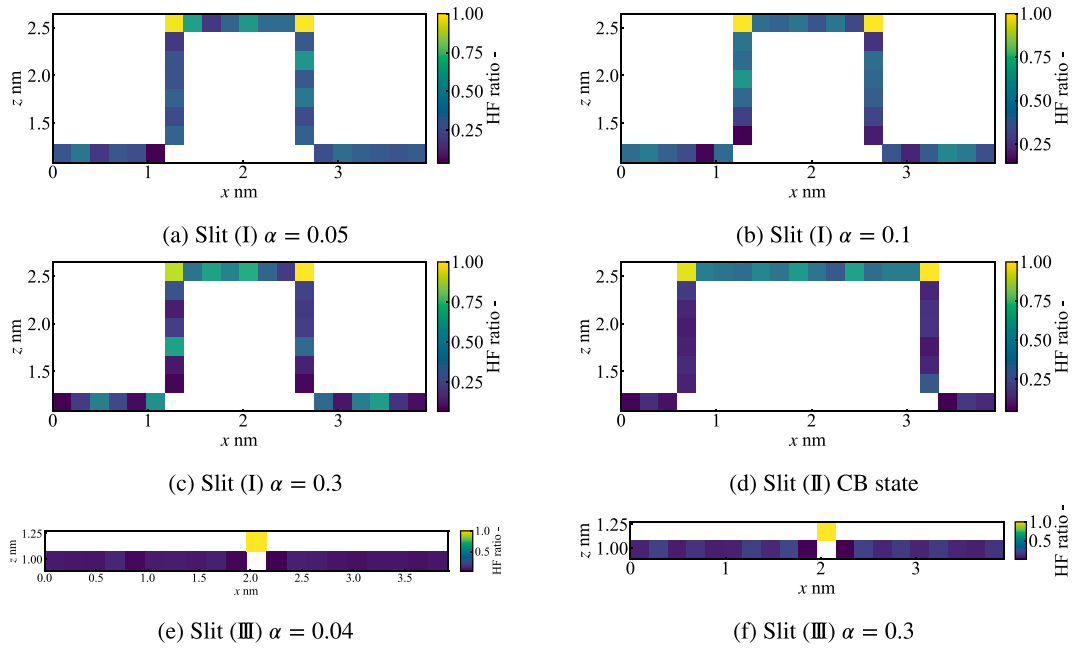

Fig. 14. Ratio of local heat flux with the maximum value set to 1.

between the bottom wall and liquid molecules in the case of Slit (II) is set to 0.05, thermal transport becomes small generally compared to the case of larger α as in the case of $\alpha = 0.1$ or $\alpha = 0.3$. In the case of Slit (III), the Max/Min ratio became larger when $\alpha = 0.3$ than when $\alpha = 0.04$. We consider this is because the magnitude of local heat flux depends on the adsorption state of liquid molecules rather than on structural features such as the top corner or base due to the extremely small structure. As shown in Fig. 13, it can be seen that the VDOS overlap between solid and liquid has the largest common frequency region in the case of $\alpha = 0.3$ due to the extremely high interaction strength. In this condition, liquid molecules strongly adsorbed to the solid wall, thus those absorbed molecules vibrate in more solid–like manner around the interface rather than move freely like those in the bulk liquid. These adsorbed liquid molecules consequently cause the molecular density fluctuation along the interface as demonstrated in Fig. 5. Due to these fluctuations, the heat flux fluctuation becomes large at the local interfaces and the Max/Min ratio of the local heat flux ends up increasing.

As exhibited in Fig. 15, we defined the group of local interfaces as the specific local region to investigate the impact of local thermal transports to the total thermal transport at the entire interface. The contribution of local thermal transport at each local area is shown in Fig. 16. In the calculations of the contribution shown in Fig. 16, "Top corner" includes two local areas: right and left top corners and other local areas (indicated as "Bottom left", "Side left", "Top", "Side right", or "Bottom right" in Fig. 16) consist of six local areas in the case of Slit (II) and of 3–14 local areas. "Bottom" indicates the bottom wall of the solid "Side" demonstrates the side wall of the nanostructure without the top corners, and "Top" means the top surface of the nanostructure without the top corners. Also, "left" indicates the smaller x coordinate side to the nanostructure and "right" means the larger x coordinate side. In the case of Slit (III), "Adatom" indicates the local interface at the adatom and "Others" refers to all local interfaces except the adatom. In Fig. 16, we can recognize that the top corner makes an approximately 15% contribution to the total thermal transport in all cases of Slit (I) and Slit (II). In the case of Slit (II), Fig. 16 indicates a larger contribution compared to the case of Slit (I), which reached almost 20%. This suggests that the top corner becomes more important to the thermal transport at the entire interface than the bottom or side walls. In the case of Slit (II), due to the small α and the short distance between the nanostructures, the local thermal transport of the bottom and side walls became extremely small. Consequently, the contribution of local thermal transport via top corners became large. Similarly, the top surface also had an immense contribution in the case of Slit (II). In the case of Slit (III) $\alpha = 0.04$, the adatom has more than a 35% contribution to the total thermal transport. This indicates that even a small nanostructure, comprising a single row of solid atoms, has a significant influence on the interfacial thermal transport. From these results, we confirmed that the top surface of the nanostructure including top corners or adatoms which have unique vibrational characteristics became essential for the nano–scale thermal transport in the case of the CB state where local ITRs are relatively large.

Table 3
Heat flux maximum–minimum ratio.

	Max/Min
Slit (I) $\alpha = 0.05$	25.0
Slit (I) $\alpha = 0.1$	7.02
Slit (I) $\alpha = 0.3$	14.5
Slit (II) CB state	21.7
Slit (III) $\alpha = 0.04$	36.1
Slit (III) $\alpha = 0.3$	67.3

4. Conclusions

In the present study, we have investigated the distributions of the local ITRs at a nanostructured solid–liquid interface using NEMD simulations, including the case of the CB state and an extremely high interaction strength between solid atoms and liquid molecules. We employed surfaces with cuboid nanostructures of various sizes. To obtain basic information on the local ITR distributions in detail, we have investigated the VDOS and SHF at each local interface and revealed the relationship between the local vibrational properties and the local ITRs. It was verified that the local ITRs increased at the base of the nanostructure and decreased at the top corner of it independent of the interaction strength between solid atoms and liquid molecules, the CB state, and the size of the nanostructure. Considering the local thermal transport per the local interface, the top corner and the adatom

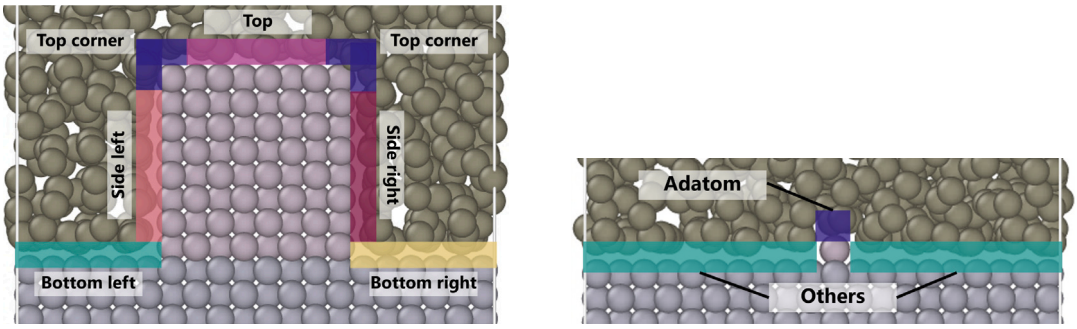

(a) Slit (Ⅰ) and Slit (Ⅱ) (b) Slit (Ⅲ)

Fig. 15. Definitions of local region in the calculation of contribution of local thermal transport.

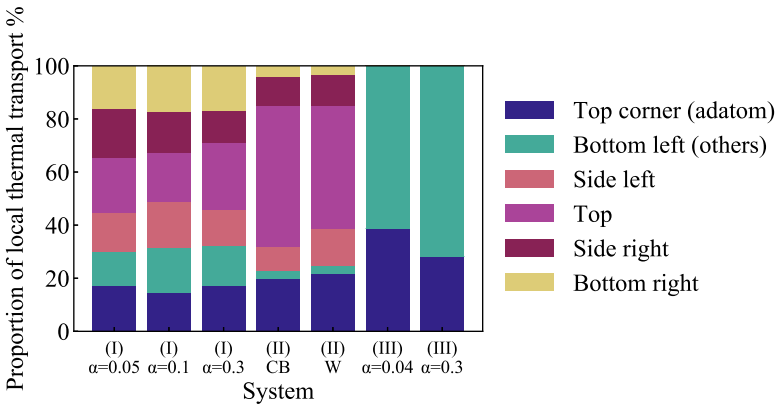

Fig. 16. Contribution of local thermal transport of local areas to overall thermal transport.

contributed considerably to the total thermal transport at the entire interface. We have also computed the combined local ITRs based on the TCM. The ratio of the overall ITR to the combined local ITRs agreed with the ratio of the area of the flat surface to the area along the lower wall and the nanostructure only when the assumption of a parallel thermal circuit holds; that is, the interaction strength between solid atoms and liquid molecules is not extremely high, regardless of whether the system is in the W or CB states. In the case of an extremely high interaction strength, liquid molecules near the interface are strongly adsorbed to the solid wall, and they caused fluctuations of the local temperature difference at the interface. The assumption of the TCM requires uniformity of the local temperature jump. Therefore, when the variance of the local temperature jump is relatively consistent, we find that the ITR ratio agrees with the area ratio within certain errors regardless of the size of the nanostructure.

Furthermore, through an analysis of vibrational properties, we have found that the local VDOS of solid atoms and SHF had a peak of 2 THz only at the top corner and the adatom, except for the case of the extremely high interaction strength between solid atoms and liquid molecules. In that case, the local VDOS of the liquid shifted to the high–frequency side. Also, the local VDOS overlap between solid and liquid indicated that the top corner and adatom had the largest value among those at other local interfaces. The results of the SHF analysis indicated that the influence of the top corners on the overall energy transport became more pronounced in the case of the CB state compared to the W state. The VDOS overlap between solid and liquid also endorsed the results since the vibrational coupling was the strongest at the top corner.

These results illustrate the importance of the distribution of local thermal resistances at a solid–liquid interface. Regardless of whether liquid molecules fill between the nanostructures, it is possible to manipulate an overall ITR by varying the interaction strength and the size of the nanostructure.

CRediT authorship contribution statement

Takuto Omori: Writing – original draft, Validation, Software, Methodology, Investigation, Formal analysis, Data curation, Conceptualization. **Masahiko Shibahara:** Writing – review & editing, Resources, Project administration, Investigation, Conceptualization.

Declaration of competing interest

The authors declare the following financial interests/personal relationships which may be considered as potential competing interests: Takuto Omori reports financial support was provided by Japan Society for the Promotion of Science. If there are other authors, they declare that they have no known competing financial interests or personal relationships that could have appeared to influence the work reported in this paper.

Acknowledgments

This work was supported by the Japan Society for the Promotion of Science (JSPS), “Grant –in–Aid for Science Research No. 23H01355”.

Data availability

Data will be made available on request.

References

[1] Z. Li, Q. Cao, Z. Cui, Enhanced heat transfer of liquid film evaporation via subdividable patterned surfaces, J. Mol. Liq. 391 (2023) 123404, http://dx.doi.org/10.1016/j.molliq.2023.123404.

[2] J. Calame, R. Myers, S. Binari, F. Wood, M. Garven, Experimental investigation of microchannel coolers for the high heat flux thermal management of GaN-on-SiC semiconductor devices, Int. J. Heat Mass Transfer 50 (23) (2007) 4767–4779, http://dx.doi.org/10.1016/j.ijheatmasstransfer.2007.03.013.

[3] H. Dang, Q. Zhang, Y. Lu, X. Zhang, W. Ma, X. Zhang, Optimizing the heat source layout of chips using bionic method: Reduction of junction temperature, Int. J. Heat Mass Transfer 197 (2022) 123321, http://dx.doi.org/10.1016/j.ijheatmasstransfer.2022.123321.

[4] Z. Lu, K.L. Wilke, D.J. Preston, I. Kinefuchi, E. Chang-Davidson, E.N. Wang, An ultrathin nanoporous membrane evaporator, Nano Lett. 17 (10) (2017) 6217–6220, http://dx.doi.org/10.1021/acs.nanolett.7b02889.

[5] D.F. Hanks, Z. Lu, J. Sircar, T.R. Salamon, D.S. Antao, K.R. Bagnall, B. Barabadi, E.N. Wang, Nanoporous membrane device for ultra high heat flux thermal management, Microsyst. Nanoeng. 4 (1) (2018) http://dx.doi.org/10.1038/s41378-018-0004-7.

[6] D.F. Hanks, Z. Lu, J. Sircar, I. Kinefuchi, K.R. Bagnall, T.R. Salamon, D.S. Antao, B. Barabadi, E.N. Wang, High heat flux evaporation of low surface tension liquids from nanoporous membranes, ACS Appl. Mater. Interfaces 12 (6) (2020) 7232–7238, http://dx.doi.org/10.1021/acsami.9b20520.

[7] C. Zhao, Y. Tao, Y. Yu, Molecular dynamics simulation of thermal and phonon transport characteristics of nanocomposite phase change material, J. Mol. Liq. 329 (2021) 115448, http://dx.doi.org/10.1016/j.molliq.2021.115448.

[8] R. Knight, D. Hall, J. Goodling, R. Jaeger, Heat sink optimization with application to microchannels, IEEE Trans. Compon. Hybrids Manuf. Technol. 15 (5) (1992) 832–842, http://dx.doi.org/10.1109/33.180049.

[9] D.G. Cahill, W.K. Ford, K.E. Goodson, G.D. Mahan, A. Majumdar, H.J. Maris, R. Merlin, S.R. Phillpot, Nanoscale thermal transport, J. Appl. Phys. 93 (2) (2003) 793–818, http://dx.doi.org/10.1063/1.1524305.

[10] P.L. Kapitza, Heat transfer and superfluidity of Helium II, Phys. Rev. 60 (1941) 354–355, http://dx.doi.org/10.1103/PhysRev.60.354.

[11] S. Merabia, J. Lombard, A. Alkurdi, Importance of viscoelastic and interface bonding effects in the thermal boundary conductance of solid–water interfaces, Int. J. Heat Mass Transfer 100 (2016) 287–294, http://dx.doi.org/10.1016/j.ijheatmasstransfer.2016.04.043.

[12] D. Becerra, J.H. Walther, H.A. Zambrano, Role of underlying substrates on the interfacial thermal transport in supported graphene nanochannels: Implications of thermal translucency, Nano Lett. 24 (39) (2024) 12054–12061, http://dx.doi.org/10.1021/acs.nanolett.4c02106.

[13] A. Ulman, Formation and structure of self-assembled monolayers, Chem. Rev. 96 (4) (1996) 1533–1554, http://dx.doi.org/10.1021/cr9502357.

[14] Z. Tian, A. Marconnet, G. Chen, Enhancing solid-liquid interface thermal transport using self-assembled monolayers, Appl. Phys. Lett. 106 (21) (2015) 211602, http://dx.doi.org/10.1063/1.4921758.

[15] O.M. Wilson, X. Hu, D.G. Cahill, P.V. Braun, Colloidal metal particles as probes of nanoscale thermal transport in fluids, Phys. Rev. B 66 (2002) 224301, http://dx.doi.org/10.1103/PhysRevB.66.224301.

[16] H. Fu, J. Chen, H. Wang, Z. Liu, H. Sørensen, A.S. Bahman, 3-D-lumped thermal network models for the reliability analysis of fan-cooled plate-fin heatsink, IEEE J. Emerg. Sel. Top. Power Electron. 11 (3) (2023) 3480–3491, http://dx.doi.org/10.1109/JESTPE.2023.3237717.

[17] M. Ishii, T. Hatakeyama, M. Ishizuka, Thermal network calculation model for phase change material with SPICE circuit simulator, J. Therm. Sci. Technol. 15 (3) (2020) http://dx.doi.org/10.1299/jtst.2020jtst0032, JTST0032–JTST0032.

[18] Y. Zhang, A. Fan, M. An, W. Ma, X. Zhang, Thermal transport characteristics of supported carbon nanotube: Molecular dynamics simulation and theoretical analysis, Int. J. Heat Mass Transfer 159 (2020) 120111, http://dx.doi.org/10.1016/j.ijheatmasstransfer.2020.120111.

[19] M. Shibahara, M. Katsuki, T. Kunugi, K. Muko, Effects of nanometer scale structure on energy transfer between a surface and fluid molecules, Nanoscale Microscale Thermophys. Eng. 10 (3) (2006) 197–204, http://dx.doi.org/10.1080/15567260600901600.

[20] X. Zhang, K. Fujiwara, M. Shibahara, Interfacial thermal resistance calculations for weak solid–liquid atom interactions using equilibrium molecular dynamics, Mol. Simul. 49 (9) (2023) 954–965, http://dx.doi.org/10.1080/08927022.2023.2202763.

[21] Y. Ueki, S. Matsuo, M. Shibahara, Molecular dynamic study of local interfacial thermal resistance of solid-liquid and solid-solid interfaces: Water and nanotextured surface, Int. Commun. Heat Mass Transfer 137 (2022) 106232, http://dx.doi.org/10.1016/j.icheatmasstransfer.2022.106232.

[22] B. Gao, Z. Zou, M. Li, M. Hao, Molecular dynamics simulation of thermal conduction across mechanical interfaces with sub-nm roughness, Int. Commun. Heat Mass Transfer 156 (2024) 107622, http://dx.doi.org/10.1016/j.icheatmasstransfer.2024.107622.

[23] M. Shibahara, K. Takeuchi, A molecular dynamics study on the effects of nanostructural clearances on thermal resistance at a lennard-jones liquid-solid interface, J. Therm. Sci. Technol. 6 (1) (2011) 9–20, http://dx.doi.org/10.1299/jtst.6.9.

[24] Y. Qu, J. Yuan, N. Deng, W. Hu, S. Wu, H. Wang, Effect of the thickness of amorphous silicon intermediate layer on the thermal transport of silicon/diamond interface, Results Phys. 52 (2023) 106827, http://dx.doi.org/10.1016/j.rinp.2023.106827.

[25] Y. Ueki, Y. Miyazaki, M. Shibahara, T. Ohara, Molecular dynamics study of thermal resistance of solid-liquid interface in contact with single layer of nanoparticles, Int. J. Heat Mass Transfer 120 (2018) 608–623, http://dx.doi.org/10.1016/j.ijheatmasstransfer.2017.12.061.

[26] K. Sääskilahti, J. Oksanen, J. Tulkki, S. Volz, Spectral mapping of heat transfer mechanisms at liquid-solid interfaces, Phys. Rev. E 93 (2016) 052141, http://dx.doi.org/10.1103/PhysRevE.93.052141.

[27] X. Wei, C.-M. Wu, Y.-R. Li, Characterizing on the interfacial thermal transport through adsorption clusters and vibrational behaviors, Int. J. Heat Mass Transfer 183 (2022) 122086, http://dx.doi.org/10.1016/j.ijheatmasstransfer.2021.122086.

[28] K. Fujiwara, S. Nakata, M. Shibahara, A spectral analysis of relationships between overall and local thermal transport across nanostructured solid-liquid interfaces, in: 7th Thermal and Fluids Engineering Conference (TFEC-2022-41157), 2022, pp. 399–408, http://dx.doi.org/10.1615/TFEC2022.emt.041157.

[29] A. El-Rifai, S. Perumanath, M.K. Borg, R. Pillai, Unraveling the regimes of interfacial thermal conductance at a solid/liquid interface, J. Phys. Chem. C 128 (20) (2024) 8408–8417, http://dx.doi.org/10.1021/acs.jpcc.4c00536.

[30] D. Surblys, Y. Kawagoe, M. Shibahara, T. Ohara, Molecular dynamics investigation of surface roughness scale effect on interfacial thermal conductance at solid-liquid interfaces, J. Chem. Phys. 150 (11) (2019) 114705, http://dx.doi.org/10.1063/1.5081103.

[31] Z. Jiang, M. Shibahara, Application of a thermal circuit model for the prediction of interfacial thermal resistance between water and a nanostructure surface using molecular dynamics simulations, Int. J. Therm. Sci. 208 (2025) 109441, http://dx.doi.org/10.1016/j.ijthermalsci.2024.109441.

[32] Y. Oki, K. Fujiwara, M. Shibahara, Molecular dynamics study of the distribution of local thermal resistances at a nanostructured solid-liquid interface, J. Therm. Sci. Technol. 19 (1) (2024) http://dx.doi.org/10.1299/jtst.24-00019.

[33] B. Smit, D. Frenkel, Vapor–liquid equilibria of the two–dimensional lennard–jones fluid(s), J. Chem. Phys. 94 (8) (1991) 5663–5668, http://dx.doi.org/10.1063/1.460477.

[34] S.-B. Zhu, M.R. Philpott, Interaction of water with metal surfaces, J. Chem. Phys. 100 (9) (1994) 6961–6968, http://dx.doi.org/10.1063/1.467012.

[35] D. Boda, D. Henderson, The effects of deviations from Lorentz–Berthelot rules on the properties of a simple mixture, Mol. Phys. 106 (20) (2008) 2367–2370, http://dx.doi.org/10.1080/00268970802471137.

[36] B. Shi, V.K. Dhir, Molecular dynamics simulation of the contact angle of liquids on solid surfaces, J. Chem. Phys. 130 (3) (2009) 034705, http://dx.doi.org/10.1063/1.3055600.

[37] L. Zhi, H. Ming, Tutorial: Determination of thermal boundary resistance by molecular dynamics simulations, J. Appl. Phys. 123 (19) (2018) 191101, http://dx.doi.org/10.1063/1.5027519.

[38] H. Matsubara, D. Surblys, Y. Bao, T. Ohara, Molecular dynamics study on vibration-mode matching in surfactant-mediated thermal transport at solid—liquid interfaces, J. Mol. Liq. 347 (2022) 118363, http://dx.doi.org/10.1016/j.molliq.2021.118363.

[39] K. Fujiwara, M. Shibahara, Atomic–scale thermal manipulation with adsorbed atoms on a solid surface at a liquid–solid interface, Sci. Rep. 9 (2019) 13202, http://dx.doi.org/10.1038/s41598-019-49677-x.